Two-Level Copper Oxide Nanostructured Surfaces for Condensation Heat Transfer

Jonggyu Lee, Bowen Shao, Yoonjin Won
University of California, Irvine
Mechanical and Aerospace Engineering
P.O. Box 6050
Irvine, CA, 92697
Email: Jonggyul@uci.edu

ABSTRACT

Condensation has been widely explored because of its importance in numerous applications including water desalination, water harvesting, and power generation. Previous studies have shown that the enhancement in condensation heat transfer can be achieved by the design of structured surfaces with desired surface chemistry. Especially, nanostructured surfaces have enhanced thermal transport performance by promoting dropwise condensation that shows lower thermal resistances than film condensation. Thus, the control of surface wettability has drawn significant interest by modulating surface morphology and surface chemistry.

In this study, we explore microscopic-level droplet dynamics using various copper surfaces. Nanostructured copper surfaces are prepared by chemical immersion methods using alkaline solution, and further functionalized by using dodecanoic acid in order to provide hydrophobicity. Their wetting properties and condensation process are investigated using an optical microscope by capturing real-time phase change process. The results show that the surface morphology with the highest feature size ratio enables to achieve the highest droplet volume growth rate due to the hindering of pinning of droplets and droplet jumping events. The understanding of condensation behaviors using the copper oxide nanostructured surfaces can provide design rules for efficient surface structures for numerous condensation applications.

KEY WORDS: dropwise condensation, copper oxide nanostructure, droplet jumping, superhydrophobic surface

NOMENCLATURE

A_s	Surface area, μm^2
d	Nanoflower diameter, m
l	Nanoneedle length, m
N	Number of droplets
P_v	Vapor pressure, Pa
P_{sat}	Saturation Pressure, Pa
r	Surface roughness
R	Droplet radius, μm
R_c	Surface contact radius, μm
T	Time, sec

Greek symbols

γ	Surface tension (N/m)
μ	Power of exponent
ϵ	Surface coverage
ϕ_s	Solid fraction
θ	Contact angle (^{o})

Subscripts

LV	liquid-vapor
SL	solid-liquid
SV	solid-vapor

Superscripts

CB	Cassie-Baxter
W	Wenzel
Y	Young-Dupre

INTRODUCTION

In recent years, controlling the wettability of solid surfaces has impacted condensation heat transfer for numerous industrial applications such as desalination [1], water harvesting [2], and power generation [3]. Typically, heat transfer coefficients for dropwise condensation are an order of magnitude larger than those for film condensation by minimizing the thermal resistance of the liquid layer. Previous studies reported that hydrophobic nanostructured surfaces lead to dropwise condensation phenomena by promoting droplet removals [4-7]. Recently, droplet coalescence induced droplet ejection or "jumping" from the condensation surface on superhydrophobic surfaces is reported [8]. In this process, two or more droplets coalescent, and extra surface energy during droplets coalescence is transferred to kinetic energy in a normal way of the surface [9]. The droplet jumping is possible through the use of suitably-designed superhydrophobic surfaces containing copper oxide nanostructures [10].

Wetting properties can be explained by three classic theories: the Young-Dupre model, Wenzel theory, and Cassie-Baxter theory. (1) The Young-Dupre model first explains that the droplet contact angle θ on a flat surface is dictated by a force balance at all the three solid-vapor, solid liquid, and liquid-vapor interfaces: $\cos\theta^Y = (\gamma_{SV} - \gamma_{SL})/\gamma_{LV}$ where γ is surface tension. In order to explain the surface roughness r impacts on the droplet formation, (2) the Wenzel equation shows that contact angle on rough surfaces is defined by [11]:

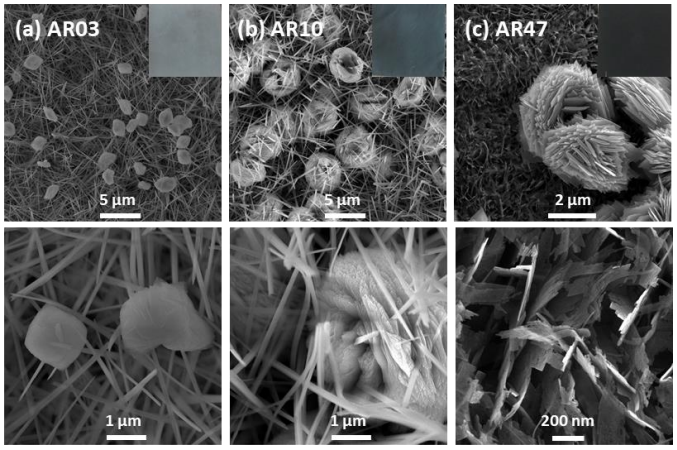

Fig. 1 Scanning electron microscope (SEM) images of nanostructured copper surfaces. (a) Nanoneedles with small nanoflowers (AR03), after 5 min immersion at room temperature. (b) Nanoneedles with nanoflowers (AR10), after 25 min immersion at room temperature. Extra immersion time affects only nanoflowers sizes rather than nanoneedle structures. (c) Small nanoneedles with nanoflowers (AR47), after 5 min immersion at 60°C.

$\cos\theta^W = \mathrm{r} \times \cos\theta^Y$, where r is the roughness which is the ratio of the total surface area to the projected area. This explains that hydrophobic surfaces become more hydrophobic whereas hydrophilic surfaces become more hydrophilic as surface roughness increases. In this case, the droplet will completely wet the rough surfaces, resulting in pinned droplets. Considering the case where the droplet rests on the tip of nanostructures, (3) the Cassie-Baxter theory introduces air gap between droplets and the surface [12]: $\cos\theta^{CB} = \phi_s(cos\theta^Y + 1) - 1$ where ϕ_s is solid fraction. The trapped air underneath the liquid-vapor interface helps droplets be suspended from the substrate and mobile [8, 13].

Here we demonstrate the effect of surface morphology on droplet dynamic behaviors using various copper nanostructured surfaces with the hydrophobicity for different saturation levels. In details, we develop hydrophobic nanostructured copper oxides using chemical immersion techniques. Then, the morphological details of structured surfaces will be correlated with droplet dynamics, and corresponding condensation. To be specific, the nanostructure is prone to flood caused by pinning of droplets because the flood on nanostructure is irreversible to be restored. In this study, attaining hydrophobicity will benefit the condensation heat transfer performance because of two facets: (1) The surface with large ratio of two-level feature size makes droplets easy to be removed from the condensing surface during the droplet coalescence by preventing the pinning; and (2) The droplets on the superhydrophobic surface maintains mobile mode of droplets due to the droplet jumping event.

METHOD

A nanostructured surface can be either hydrophobic or

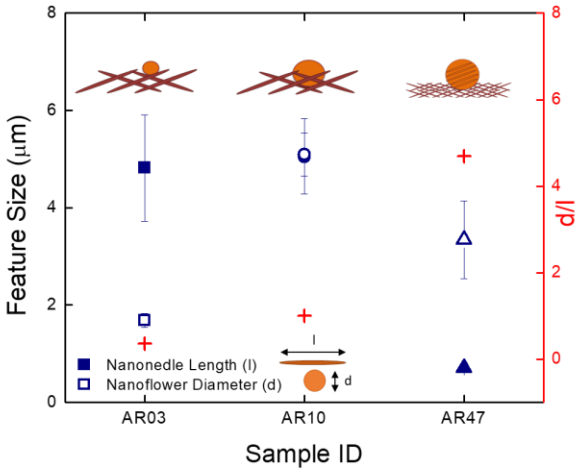

Fig. 2 Feature sizes of the AR03, AR10, and AR47 surfaces. The nanoflowers are formed with the diameter of 1.6±0.1 µm (AR03) at 5min and increase to d_2~5.1±0.5 µm (AR10) as the immersion time increases to 25 min. The nanoneedles (l_3~0.7±0.03 µm) and nanoflowers of AR47 surface oxidized in 60°C solution are smaller than nanoneedles of AR03 (l_1~4.8±1.1 µm) or AR10 (l_2~5.1±0.8 µm). Additionally, the nanoflowers are formed within nanoneedles (AR03 and AR10) where the nanoflowers (d_3~3.3±0.8 µm) are placed on the nanoneedles (AR47). The red cross shows the ratio d/l of nanoflower diameter to nanoneedle length. Error bars represent standard deviation of the measured feature size.

hydrophilic depending on chemical composition and surface roughness [14, 15]. Several techniques have been explored to modulate copper surface wettability including hydrothermal methods, electrochemical process, chemical immersion methods, or a combination of two or more methods [16, 17]. Among the different techniques, the chemical immersion method is considered a cost-effective way to roughen the surface. The morphologies of copper oxide nanostructured surfaces can be engineered by modulating chemicals, processing temperatures, and immersion time. The copper oxide nanostructured surfaces are further functionalized to increase their hydrophobicity, enabling the dropwise condensation and droplet jumping.

Surface Nanostructuring

We prepare various copper nanostructured surfaces by using the immersion method, as shown in scanning electron microscope (SEM) images in Fig. 1. All the samples are prepared in a size of 10 mm×10 mm×0.5 mm. Before nanostructuring process, copper substrates (99.9%, pure, McMaster-Carr) are cleaned with acetone, methanol, and isopropanol and rinsed with 2M HCl and DI water. Then, the copper substrates are oxidized using the chemical solution of a

Table 1. Feature sizes and aspect ratio of nanoflower diameter to nanoneedle length of AR03, AR10, and AR47 surfaces.

	AR03	AR10	AR47
Apparent Ratio (AR)	0.3	1.0	4.7
Nanoneedle Length (l, μm)	4.82±1.1	5.06±0.77	0.71±0.03
Nanoflower Diameter (d, μm)	1.68±0.14	5.09±0.44	3.34±0.8

0.1M $K_2S_2O_8$ and a 2M NaOH, creating copper oxide nanostructured surfaces. The morphology of the surfaces include nanoneedle-like features and/or nanoflowers-like features, depending on the immersion time and temperature. The chemical process at room temperature (25°C) for 5 min provides the features of nanoneedles (l_1~4.8±1.1 μm) and small nanoflowers (d_1~1.6±0.1 μm) (Fig. 1a). As the process time increases up to 25 min, the nanoflowers size is increased to d_2~5.1±0.5 μm whereas the nanoneedle size remains a constant. whereas the nanoneedle size remains a constant. The chemical process at an elevated temperature at 60°C for 5 min provides the features of nanoflowers (d_3~3.34±0.8μm) and nanoneedles (l_3~0.7±0.03 μm). The feature size and shape of nanostructures are listed in Fig. 2 and Table 1. Prepared samples are named as AR03, AR10, and AR47 where "AR" means the apparent size ratio of nanoflower diameter to nanoneedle length (d/l). The average of the features is measured using a commercial software, ImageJ.

Surface Wettability

The engineered nanostructured surfaces consisting of $Cu(OH)_2$ and CuO first show hydrophilicity as shown in Fig. 3. The hydrophilic surfaces are further functionalized by using 5 mM of dodecanoic acid for 30 min. This surface treatment decreases the surface energy, resulting in surface hydrophobicity, while it maintains the copper oxide morphology. As shown in Fig. 3, the contact angle of the functionalized surfaces increases as the ratio between nanoneedle length to nanoflower diameter increases. The AR03 and AR10 show the contact angles of 136° and 148°, respectively [18]. Furthermore, the AR47 surface presents superhydrophobicity by possessing the contact angle of 165°, which is attributed to a large aspect ratio between nanoflowers and nanoneedles.

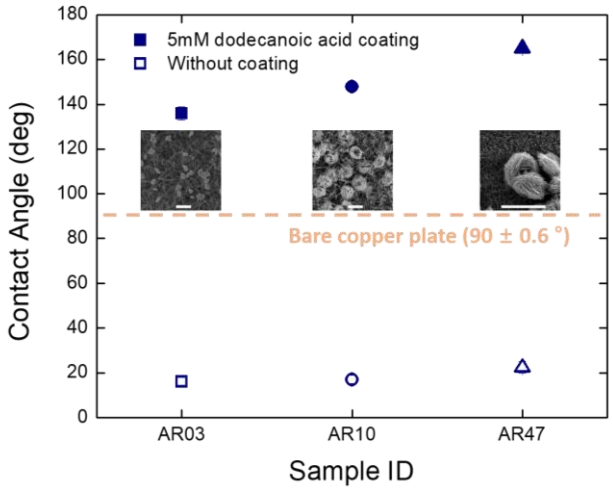

Fig. 3 Contact angles of the nanostructured copper surfaces before and after dodecanoic acid coating. The scale bar of the inset SEM image is 5 μm.

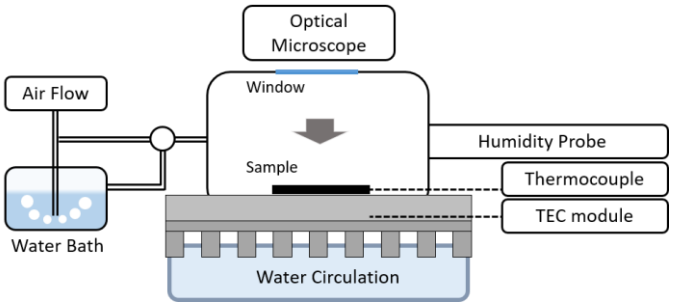

Fig. 4 1 Schematic diagram of the custom condensation measurement setup. The condensation setup is composed of humidity provider, temperature controller, and data acquisition system. Optical microscope is used to record time-lapse images during condensation test.

Dropwise Condensation Tests

Condensation behaviors are observed by using a custom-made condensation measurement setup as illustrated in Fig. 4. The condensation setup includes a chamber, thermoelectric temperature controller with DC power supply, and vapor generator. The vapor generator controls relative humidity in the condensing chamber by flowing air through the water and mixing with ambient air. The condensation conditions are controlled by the combination of relative humidity and surface temperature using thermoelectric cooling (TEC) module. Thermocouples are mounted between the sample and carbon tape to confirm a constant surface temperature during the condensation test. Microdroplet growth behaviors under the high supersaturation level (S=2.48, T_s=4°C, and P_v=2140 Pa) and low supersaturation level (S=1.09, T_s=15°C, and P_v=1873 Pa) are explored. In this process, the supersaturation is defined as P_v/P_{sat} where P_{sat} is saturation pressure at the surface temperature T_s. The droplet behaviors are recorded from the top view through a window using an optical microscope [19]. The number and diameter of droplets are analyzed by image processing from top view microscope images.

RESULTS AND DISCUSSION

Characterization of Dropwise Condensation

In order to analyze the dropwise condensation, we measure the droplet growth behaviors by recording condensation images using the optical microscope. The time-lapse optical images are

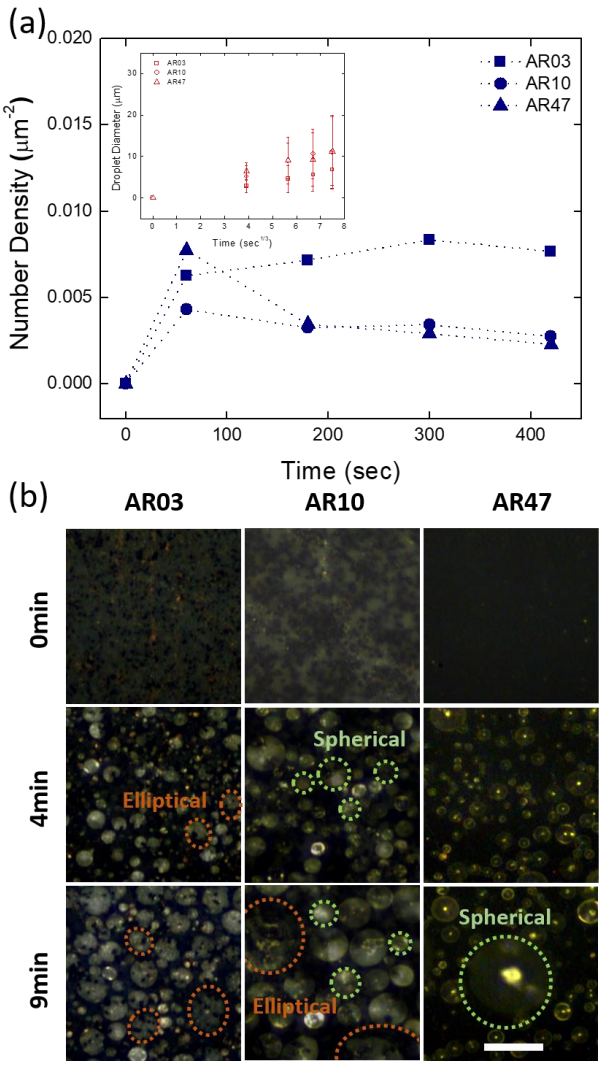

Fig. 5 (a) The number density and droplet diameter (inset) at the high supersaturation (S=2.48). The navy dot lines are trend line of each point of the droplet number density. Square, circle, and triangle represent the AR03, AR10, and AR47, respectively. The error bar represents a standard deviation of the measured droplet size. (b) Time-lapse optical images (top view) of the surfaces at S=2.48, and P_v=2140 Pa. Each column shows the AR03, AR10, and AR47 surfaces. The orange, green, and red line represent elliptical shape and spherical shape, respectively. The scale bare is 50 μm.

used to obtain the condensation behaviors at S=2.48 and P_v=2145 Pa for the AR03, AR10, and AR47 surfaces (225 μm×160 μm) at different time frames as shown in Fig. 5. The images allow us to evaluate the droplet number density, diameter, and shape as the condensation time increases for different surface structures as indicated in Fig. 5(a). The droplet number density of AR03 at S=2.48 consistently shows an increase up to 0.0062 μm^{-2} and remains a constant. The droplet number density decreases during condensation as droplets coalesce. Thereby, a consistent number density is observed because the low condensation rate hinders the droplet coalescence events. On the other hand, the number density of AR10 or AR47 surfaces decays. The low number density of droplets leads to a small surface coverage by droplets during the condensation process lowering thermal resistance [13].

The time-lapse optical images in Fig 5(b) show the droplet coalescence or jumping phenomena by indicating the differences in droplet shapes on the condensing surfaces. Droplet shapes such as spherical or elliptical shapes can suggest the droplet status. For example, initial droplets on hydrophobic surfaces are prone to be spherical shapes. Here, if the droplets are not pinned or suspended from the original position, the state of a droplets is defined as a mobile mode. When the droplets coalesce, the combined droplets will remain the same spherical shapes. Instead, the new shape of the combined droplets will be elliptical since some portion of droplets is still pinned on the nanostructured surface. In Fig. 5(b), we consistently observe elliptical-shaped droplets since the early stage of condensation (at 4 min) on the AR03 while elliptical-shaped droplets generate at ~9 min. The presence of elliptical shapes might be attributed to the combination of the hydrophobicity (contact angles; 136°-148°, Fig. 3) and morphological differences (length; 3.7 ~5.9 μm, Fig. 2). The superhydrophobicity of the AR47 surface enables droplet jumping events. Once the droplet jumping events happen, they open up more spaces to promote new droplet nucleation sites.

It has been challenging to observe the details of droplet phenomena at S=2.48 due to small droplet sizes. Therefore we repeat the condensation measurement using a low supersaturation level at S=1.09 for a longer time period of 90 min. The general trends in the droplet number density and diameter at S=1.09 show a good agreement with the measurements at S=2.48. As the condensation time increases, droplet number density increases first until 10 min and rapidly decays after droplets start to coalesce. In the early stage of condensation (10 min), the droplet number density of the AR03 (2.3×10^{-3} μm^{-2}) is larger than those of the AR10 and AR47 surfaces (5.2×10^{-4} μm^{-2} and 1.4×10^{-3} μm^{-2}, respectively) as shown in Fig 6(a). The number density of the AR10 remains a constant due to the absence of droplets coalescence whereas that of AR47 fluctuates due to droplet jumping and nucleation cycling.

The detailed optical images in Fig 6(b) show dropwise condensation and droplet jumping phenomena on the AR03, AR10, and AR47 surfaces at S=1.09. The transition from sphere shape-dominated regime to elliptic shape-dominated regime appears after 10 min and 70 min for AR03 and AR10, respectively, confirming the pinned droplet status. Spherical-shaped droplets on the AR47 surface confirm mobile mode, leading to droplet jumping events in the later stages [10]. Once droplets jump, they provide extra spaces to enable new nucleation sites whereas it is difficult to observe new nucleation sites on other surfaces.

The changes in droplet sizes during the condensation are

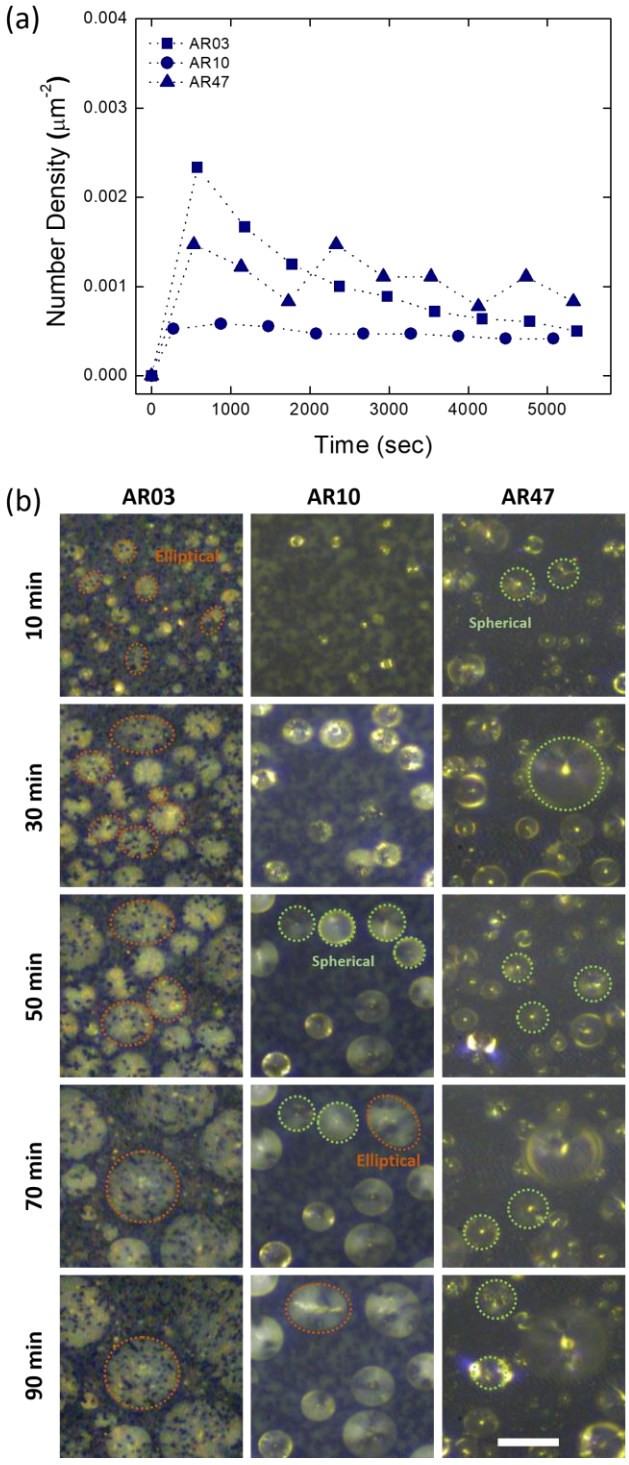

Fig. 6 (a) The droplet number density at the low supersaturation (S=1.09). The navy dot lines show the trend of the droplet number density. (b) Optical microscope images showing droplet dynamics at S=1.09 and P_v=1882 Pa. Time-lapse optical images suggest droplet growing and coalescence behavior. The scale bar is 50 μm.

analyzed by using a power law of droplet growth, $R = at^{\mu}$, where R is the droplet radius, t is the time, a is a constant, and

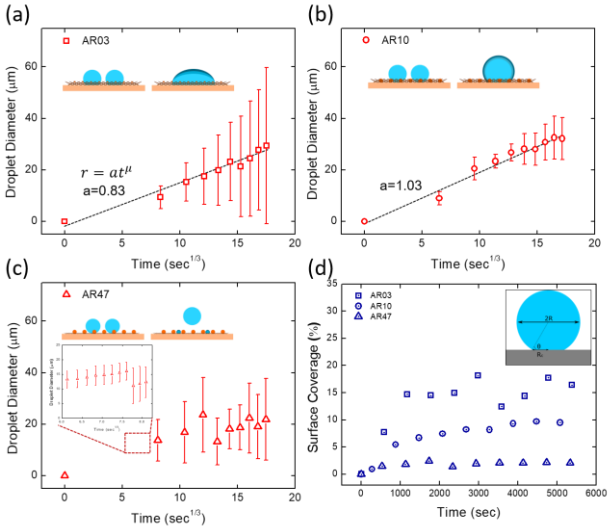

Fig. 7 Droplet diameter at the low supersaturation S=1.09 for (a) AR03, (b) AR10, and (c) AR47. Constants of the power law for droplet growth model, $R=at^{\mu}$ at a low saturation are calculated where μ=1/3. The black dash line is calculated by using the least square of the droplet diameters. Error bars represent the standard deviation of droplet diameter. (d) Surface coverage by the droplets. The surface coverage is calculated by using droplet diameters and apparent contact angles.

μ is a power of exponent. The power of exponent μ is known as 1/3 [20]. The values of a can be calculated by the least square from droplet diameter in Fig. 7 where a large constant a value means that the fast increase rate of a droplet diameter . Error bars of the droplet diameter shows the standard deviations of droplet diameters on the condensing surface. The droplet coalescences on the AR03 cause the fast increase in droplet diameter as well as large error bars. On the other hand, most droplets are prone to grow and some droplets coalescence, leading to small error bars. The trend of droplet diameters of the AR47 fluctuates during the condensation, confirming the droplet jumping events.

We identify the surface coverage of droplets to determine the surface favorable to dropwise condensation. As the droplet size increases, the surface coverage by droplets increases. The surface coverage is determined by following equation:

$$R_c = R\cos(\theta - \frac{\pi}{2}) \quad (1)$$

$$\epsilon = \frac{\pi R_c^2 N}{A_s} \quad (2)$$

where R_c is the surface contact radius at the bottom of droplets, θ is the apparent contact angle, N is the number of droplets, ϵ is the surface coverage ratio, and A_s is the condensing surface area measured to calculate droplet number density and diameter (225 μm×160 μm). As shown in Fig 7(d), the droplets on the AR03 cover a larger surface area whereas the surface coverage of the AR47 surface is relatively small due to the droplet

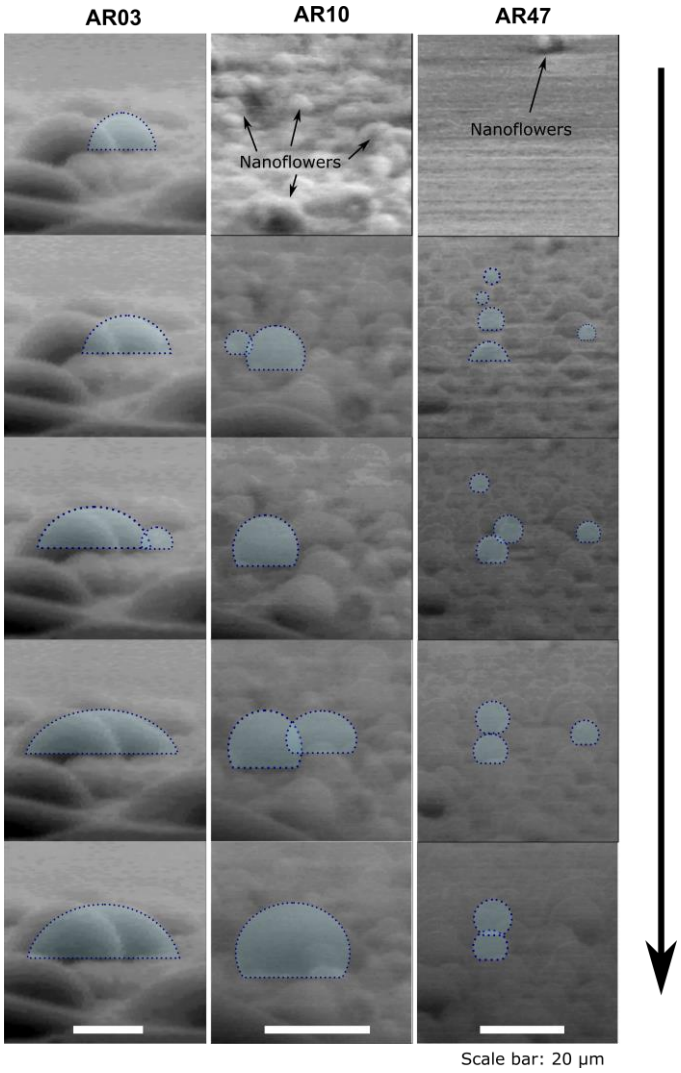

Fig. 8 Environmental scanning electron microscope (ESEM) images showing droplet shape change on nanostructured surfaces. The increase in surface contact areas and the decrease in contact angles are observed due to pinned mode of droplets for the AR03 surface. Most droplets on the AR10 and AR47 surfaces show spherical shapes. The scale bar is 20 μm.

jumping.

In order to examine droplet shapes at the microscale-level, we capture environmental scanning electron microscope (ESEM) images, as shown in Fig. 8. In this process, the presence of nanostructures has limited the direct observation of the droplet pinning at the surface. Instead, the changes in droplet shape and contact angle during droplet coalescence can be observed. The elliptic shape of droplets (i.e., pinned droplets) results in a large surface coverage and the decrease in contact angles of the AR03 surface. For the AR10 surface, droplets first show small spherical droplets (<20 μm) at the early stage and then become elliptic droplets as droplet size increases. The droplets on the AR47 superhydrophobic surface exist as both suspended and partially wetted at the early stage.

Based on the condensation performance obtained using the AR03, AR10, and AR47 surfaces, we understand the effects of hydrophobic surfaces' morphology on droplet growth behavior. The hierarchy of copper oxide nanostructure provides the promising surface morphology in terms of desirable wetting properties and corresponding droplet status for dropwise condensation. It would be interesting for the future research to explore the relationship between initial pinning area of droplets and nucleation density, which is crucial to determine effective radius of droplets and initial contact angle change [6].

CONCLUSION

In summary, we study dynamic droplet behaviors under condensation by using various surface morphologies. The hierarchy of copper oxide nanostructure provides the promising surface morphology in terms of desirable wetting properties and droplet status. For this, the copper substrates are oxidized using the chemical immersion method and further functionalized using the dodecanoic acid to become hydrophobic. Key findings from the study are as follows: (1) The combination of small feature size of nanoneedles and large aspect ratio of two-level features enhances the surface hydrophobicity. (2) Hydrophobic surfaces (i.e., AR03 and AR10) show both pinned mode and mobile mode of droplets under the condensation regime. (3) Superhydrophobic surface through the large hierarchy of copper oxide nanostructures (i.e., AR47) facilitates the mobile mode of droplets, enabling droplet jumping events, a small surface coverage, and thereby a minimum thermal resistance. We envision that condensation study of the nanostructured copper surface with different morphology broadens the design principle of hierarchical structures for applications ranging from condensation heat transfer to water collecting surfaces.

ACKNOWLEDGEMENT

J.L. is thankful for the financial support from the UCI Mechanical and Aerospace Engineering Department Graduate Fellowship.

REFERENCES

[1] A. D. Khawaji, I. K. Kutubkhanah, and J.-M. Wie, "Advances in seawater desalination technologies," *Desalination,* vol. 221, no. 1-3, pp. 47-69, 2008.

[2] H. G. Andrews, E. A. Eccles, W. C. Schofield, and J. P. Badyal, "Three-dimensional hierarchical structures for fog harvesting," *Langmuir,* vol. 27, no. 7, pp. 3798-802, 2011.

[3] J. M. Beér, "High efficiency electric power generation: The environmental role," *Progress in Energy and Combustion Science,* vol. 33, no. 2, pp. 107-134, 2007.

[4] C.-H. Chen *et al.*, "Dropwise condensation on superhydrophobic surfaces with two-tier roughness," *Applied Physics Letters,* vol. 90, no. 17, p. 173108, 2007.
[5] C. Dietz, K. Rykaczewski, A. G. Fedorov, and Y. Joshi, "Visualization of droplet departure on a superhydrophobic surface and implications to heat transfer enhancement during dropwise condensation," *Applied Physics Letters,* vol. 97, no. 3, p. 033104, 2010.
[6] S. Kim and K. J. Kim, "Dropwise Condensation Modeling Suitable for Superhydrophobic Surfaces," *Journal of Heat Transfer,* vol. 133, no. 8, p. 081502, 2011.
[7] P. G. A. Umur, "Mechanism of Dropwise Condensation," *Journal of Heat Transfer,* 1965.
[8] R. Enright, N. Miljkovic, J. Sprittles, K. Nolan, R. Mitchell, and E. N. Wang, "How coalescing droplets jump," *ACS Nano,* vol. 8, no. 10, pp. 10352-62, 2014.
[9] R. Enright, N. Miljkovic, N. Dou, Y. Nam, and E. N. Wang, "Condensation on Superhydrophobic Copper Oxide Nanostructures," *Journal of Heat Transfer,* vol. 135, no. 9, p. 091304, 2013.
[10] N. Miljkovic, R. Enright, and E. N. Wang, "Effect of droplet morphology on growth dynamics and heat transfer during condensation on superhydrophobic nanostructured surfaces," *ACS Nano,* vol. 6, no. 2, pp. 1776-85, 2012.
[11] R. N. Wenzel, "Resistance of Solid Surfaces to Wetting by Water," *Industrial and Engineering Chemistry,* vol. 28, no. 988-994, 1936.
[12] A. B. D. Cassie and S. Baxter, "Wettibility of porous surfaces," *Transactions of the Faraday Society,*vol. 40, pp. 546-551, 1944.
[13] D. W. DTanner, C. J. Potter, D. Pope, and D. West, "Heat transfer in dropwise condensation-PART 1: The effects of heat flux, steam velocity and non-condensable gas concentration," *Int. J. Heat Mass Transfer,* vol. 8, pp. 419-426, 1965.
[14] K. Rykaczewski *et al.*, "How nanorough is rough enough to make a surface superhydrophobic during water condensation?," *Soft Matter,* vol. 8, no. 33, p. 8786, 2012.
[15] W. Choi, A. Tuteja, J. M. Mabry, R. E. Cohen, and G. H. McKinley, "A modified Cassie-Baxter relationship to explain contact angle hysteresis and anisotropy on non-wetting textured surfaces," *J Colloid Interface Sci,* vol. 339, no. 1, pp. 208-16, 2009.
[16] S. Wang, L. Feng, and L. Jiang, "One-Step Solution-Immersion Process for the Fabrication of Stable Bionic Superhydrophobic Surfaces," *Advanced Materials,* vol. 18, no. 6, pp. 767-770, 2006.
[17] D.-J. Huang and T.-S. Leu, "Fabrication of high wettability gradient on copper substrate," *Applied Surface Science,* vol. 280, pp. 25-32, 2013.
[18] J. Tian, Y. Zhang, J. Zhu, Z. Yang, and X. Gao, "Robust nonsticky superhydrophobicity by the tapering of aligned ZnO nanorods," *Chemphyschem,* vol. 15, no. 5, pp. 858-61, 2014.
[19] H. Kim and Y. Nam, "Condensation behaviors and resulting heat transfer performance of nano-engineered copper surfaces," *International Journal of Heat and Mass Transfer,* vol. 93, pp. 286-292, 2016.
[20] J. W. Rose and L. R. Glicksman, "Dropwise condensation-The distribution of drop sizes," *International Journal of Heat Mass Transfer,* vol. 16, pp. 411-425, 1973.